International Journal of Nanomedicine

Dovepress
open access to scientific and medical research

Open Access Full Text Article

ORIGINAL RESEARCH

Biocompatibility, endocytosis, and intracellular trafficking of mesoporous silica and polystyrene nanoparticles in ovarian cancer cells: effects of size and surface charge groups

This article was published in the following Dove Press journal:
International Journal of Nanomedicine
30 July 2012
Number of times this article has been viewed

Maneerat Ekkapongpisit[1]
Antonino Giovia[1]
Carlo Follo[1]
Giuseppe Caputo[2,3]
Ciro Isidoro[1]

[1]Laboratory of Molecular Pathology and Nanobioimaging, Department of Health Sciences, Università del Piemonte Orientale "A Avogadro", Novara, [2]Dipartimento di Chimica dell'Università di Torino, Torino, [3]Cyanine Technology SpA, Torino, Italy

Background and methods: Nanoparticles engineered to carry both a chemotherapeutic drug and a sensitive imaging probe are valid tools for early detection of cancer cells and to monitor the cytotoxic effects of anticancer treatment simultaneously. Here we report on the effect of size (10–30 nm versus 50 nm), type of material (mesoporous silica versus polystyrene), and surface charge functionalization (none, amine groups, or carboxyl groups) on biocompatibility, uptake, compartmentalization, and intracellular retention of fluorescently labeled nanoparticles in cultured human ovarian cancer cells. We also investigated the involvement of caveolae in the mechanism of uptake of nanoparticles.

Results: We found that mesoporous silica nanoparticles entered via caveolae-mediated endocytosis and reached the lysosomes; however, while the 50 nm nanoparticles permanently resided within these organelles, the 10 nm nanoparticles soon relocated in the cytoplasm. Naked 10 nm mesoporous silica nanoparticles showed the highest and 50 nm carboxyl-modified mesoporous silica nanoparticles the lowest uptake rates, respectively. Polystyrene nanoparticle uptake also occurred via a caveolae-independent pathway, and was negatively affected by serum. The 30 nm carboxyl-modified polystyrene nanoparticles did not localize in lysosomes and were not toxic, while the 50 nm amine-modified polystyrene nanoparticles accumulated within lysosomes and eventually caused cell death. Ovarian cancer cells expressing caveolin-1 were more likely to endocytose these nanoparticles.

Conclusion: These data highlight the importance of considering both the physicochemical characteristics (ie, material, size and surface charge on chemical groups) of nanoparticles and the biochemical composition of the cell membrane when choosing the most suitable nanotheranostics for targeting cancer cells.

Keywords: nanoparticles, imaging, lysosomes, vesicular traffic, ovarian cancer, caveolin

Introduction

Ovarian cancer is the fifth leading cause of cancer-related deaths among women, and the most lethal of the gynecological cancers.[1] The high mortality rate in patients with ovarian cancer is primarily attributable to late diagnosis, when metastases have already formed, and to development of chemoresistant clones that eventually cause relapse.[2] In addition to an intrinsic inability to activate a cell death program,[3,4] mechanisms of chemoresistance in cancer cells include lysosomal sequestration and inactivation,[5] and enhanced efflux of the toxic drug.[6,7] Given the silent nature of the development of ovarian cancer and its extreme lethality, there is an urgent need to develop sensitive

Correspondence: Ciro Isidoro
Università del Piemonte Orientale "A Avogadro", Dipartimento di Scienze della Salute, Via Solaroli 17, 28100 Novara, Italy
Tel +39 03 2166 0607
Fax +39 03 2162 0421
Email isidoro@med.unipmn.it

methods for early diagnosis of primary and secondary lesions and novel strategies to deliver cytotoxic drugs to chemoresistant clones.

Theranostic nanoparticles engineered to carry both a chemotherapeutic drug and a sensitive imaging probe allow simultaneous detection of cancer cells and monitoring of the cytotoxic effects of anticancer treatment.[8–10] Further, such nanocarriers can overcome chemoresistance by circumventing activation of extruding mechanisms and by protecting the drug from lysosomal degradation.[11,12] Nanoparticles can reach and accumulate within the tumor site passively, exploiting leaky and imperfect tumor neovascularization and defective lymphatic drainage,[13,14] or actively, by functionalizing the surface of the nanoparticles with ligands specifically directed to targets expressed on tumor cells.[15–18]

Before a nanomaterial can be deemed a suitable theranostic tool, it is necessary to assess its ability to enter the cell, to reach the desired intracellular compartment (wherein the drug will be liberated), and to remain in the cell for a time period sufficient to allow adequate diagnostic and therapeutic functions. In this respect, it is convenient to select the nanoparticle first for its potential as an "in cell" imaging agent and thereafter proceed with its "upgrade' to theranostics by adding a therapeutic function. The purpose of the present work was to analyze the potential of mesoporous silica and polystyrene nanoparticles as theranostics in ovarian cancer by assessing in vitro their uptake, toxicity, and intracellular trafficking and stability. Mesoporous silica (MCM-41) nanoparticles are emerging as powerful nanotheranostic tools because of their porous structure, which allows them to host a large number of dye and drug molecules and because silica is considered to be safe and biodegradable.[19–21] While amorphous mesoporous silica nanoparticles show poor biocompatibility towards various cell types,[22–24] mobile composition matter of the MCM-41 type is well tolerated both in vitro and in vivo.[25] Polystyrene nanoparticles are also under evaluation for drug delivery and cellular imaging.[26–29]

In this work, we analyzed the mechanism of entry, intracellular trafficking, final localization, and biocompatibility of fluorescently labeled mesoporous silica and polystyrene nanoparticles differing in size and surface charge of chemical groups in ovarian cancer cells. In a first set of experiments, we compared mesoporous silica nanoparticles 10 ± 5 nm diameter, naked (ie, no surface-charged functional group), and doped with IRIS-3 dye emitting red fluorescence,[30] with commercial polystyrene nanoparticles 30 ± 10 nm in diameter, carboxyl-modified with a negative surface charge, and embedded with fluorescein isothiocyanate (FITC) dye emitting green fluorescence. In a second set of experiments, to get a preliminary insight into the impact of size and surface charge groups, we further tested the biocompatibility, uptake, and subcellular localization of mesoporous silica and polystyrene nanoparticles 50 nm in diameter and functionalized (or not) with amine or carboxyl groups.

As a cell model of human ovarian cancer, we initially chose the NIHOVCAR3 cell line, which has been shown to be resistant to a variety of chemotherapeutics,[31] and refractory to caveolin-dependent endocytosis of phospholipid-based nanocarriers.[32,33] Caveolin-1 is the principal constituent of caveolae, and acts as an oncosuppressor in ovarian cancer.[34] SKOV3, a human ovarian cancer cell line, has been shown to be able to take up various types of nanoparticles in a caveolin-1-dependent manner. Therefore, the SKOV3 cell line was used for the second series of experiments. Schematically, we found that: nanoparticles exploited different mechanisms of entry, followed different endocytic routes, and showed different cellular compartmentalization depending on size and type of material; 10 nm naked mesoporous silica nanoparticles showed the highest and 50 nm carboxyl-modified mesoporous silica nanoparticles showed the lowest uptake efficiency, independent of caveolin-1 expression; 30 nm carboxyl-modified polystyrene nanoparticles were biocompatible, although not retained intracellularly for a long time, and did not enter the acidic endocytic pathway, whereas 50 nm amine-modified polystyrene nanoparticles accumulated in lysosomes and were toxic. Uptake of 10 nm mesoporous silica nanoparticles was not affected by serum, whereas 30 nm polystyrene nanoparticles was thus affected.

Materials and methods

Nanoparticles

The following commercial polystyrene nanoparticles were purchased from Sigma-Aldrich (St Louis, MO): 1000 nm polystyrene nanoparticles, amine-functionalized, red color-conjugated (L2778); 50 nm polystyrene nanoparticles, amine-functionalized, blue color-conjugated (L0780); and 30 nm polystyrene nanoparticles, carboxyl-functionalized and FITC-conjugated (L5155). The following mesoporous silica nanoparticles were provided by Cyanine Technologies SpA (Turin, Italy): 10 nm mesoporous silica nanoparticles, naked, engrafted with IRIS-3 (IRIS3-Dots-Porous, c3WEL-06); 50 nm mesoporous silica nanoparticles, naked, engrafted with IRIS-3 (IRIS3-Dots, 3DOT.01); 50 nm mesoporous silica nanoparticles, amine-functionalized, engrafted with IRIS-3

(IRIS Dots-3 amine, 3DOT-03); and 50 nm mesoporous silica nanoparticles, carboxyl-functionalized, engrafted with IRIS-3 (IRIS Dots-3 carboxyl, 3DOT-02).

Cell culture and treatment

Ovarian NIH-OVCAR3 and SKOV-3 cancer cells were cultivated at 37°C with 5% CO_2 in Dulbecco's modified Eagle Minimum Essential Medium (Sigma-Aldrich) supplemented with 10% fetal bovine serum (Lonza Group Ltd, Basel, Switzerland) and 100 IU/mL penicillin-streptomycin (Sigma-Aldrich). Typically, the cells were plated on sterile coverslips and allowed to adhere for 24 hours prior to use. The incubations were performed in fresh medium for the time indicated. After brief sonication to disrupt conglomerates, nanoparticles were dissolved directly in culture medium to the desired final concentration.

Cell viability assessment

Cell toxicity was evaluated by checking the metabolic activity of the cell. To this end, the cells were loaded with the nanoparticles and then labeled with CellTracker™ (Life Technologies Ltd, Paisley, UK), a fluorescent dye that emits blue fluorescence of intensity proportional to mitochondrial respiratory activity.[35] The cells were labeled with 5 μM CellTracker for 45 minutes in serum-free medium, and were then washed and incubated in regular complete medium for 30 minutes and observed under the fluorescence microscope. As a control for metabolic toxicity, the cells were incubated with 1% dimethyl sulfoxide (Sigma Aldrich). Cell viability was measured as the percentage of cells labeled with CellTracker as determined with ImageJ software.

Nanoparticle uptake and intracellular trafficking

NIHOVCAR-3 and SKOV-3 cells were plated onto sterile coverslips and allowed to adhere for 24 hours. The medium was then replaced, and the cells were incubated with the nanoparticles for the time indicated. To track the endocytic pathway, the cells were prelabeled 10 minutes beforehand with Lysotracker Green 100 nM or Red 50 nM (Life Technologies Ltd). Alternatively, cells preloaded with nanoparticles were subjected to fixation, permeabilization, and immunofluorescence staining with anti-Lamp1 antibody, which labels both endosomes and lysosomes.[36] Incubation at 4°C was performed on ice with protection from exposure to light. The chilled nanoparticles were diluted in either serum-containing or serum-free medium and added to the cells on ice for the time indicated. The cells were then brought back to 37°C for recovery, and the endocytosed nanoparticles were imaged under a fluorescent microscope (Leica DMI6000, Leica Microsystems AG, Wetzlad, Germany) at various intervals of recovery. In order to extract cholesterol from the plasma membrane, 5 mM of methyl-β-cyclodextrin (MbCD, Sigma-Aldrich) was added for 60 minutes in serum-free medium prior to incubation with the nanoparticles.

Fluorescence microscope imaging

Samples were observed with the fluorescent microscope, keeping the same settings throughout the observations. Five to ten fields (minimum 50 cells) were randomly imaged by two independent investigators (ME and AG), and representative images were chosen for display. Images were captured under the fluorescence microscope using the same color intensity threshold for all treatments. All images were compiled using Adobe Photoshop (the same contrast adjustment was applied to all images). Quantification of fluorescent microscope images was performed using the ImageJ software freely available at http://rsbweb.nih.gov/ij/.

Flow cytometry

Flow cytometry was used to determine the proportion of cells that had internalized the nanoparticles. At the end of treatment, the cells were washed three times with cold phosphate-buffered solution to remove excess nanoparticles, and extracellular fluorescence was quenched with 0.4% (w/v) Trypan blue in phosphate-buffered solution. The cells were then harvested with trypsin, resuspended in phosphate-buffered solution, and the extent of nanoparticle internalization was assessed using a FACScan flow cytometer (Becton Dickinson, Franklin Lakes, NJ). Cell-associated fluorescence (10,000 cells/sample) was analyzed with WinMID version 2.9 software.

Western blotting

The standard procedure was used for Western blotting.[36] Briefly, cell homogenates were prepared by dissolving the cells in phosphate-buffered solution containing detergents and protease inhibitors, followed by freeze-thawing and ultrasonication. Aliquots of cell homogenates were denatured in Laemmli buffer and resolved by sodium dodecyl sulfate polyacrylamide gel electrophoresis. Proteins were then transferred onto a nitrocellulose sheet and antigens revealed with a mouse monoclonal antibody against caveolin-1 (Becton Dickinson) and a monoclonal antibody against β-actin (Sigma-Aldrich), using horseradish peroxidase-conjugated secondary anti-rabbit IgG and anti-mouse IgG, respectively.

The chemoluminescent signal associated with specific bands was acquired using the VersaDoc imaging system and Quantity One software (BioRad Laboratories Inc, Hercules, CA).

Statistics

Each experiment was performed in triplicate and reproduced at least three times. Quantification data from ImageJ and cytofluorometry analyses are shown as the average ± standard deviation. The Student's *t*-test with $P < 0.05$ for statistical significance was used to compare the results from different treatments.

Results

First, we checked whether 10 nm naked mesoporous silica and 30 nm carboxyl-modified polystyrene nanoparticles were toxic to human ovarian cancer cells. No obviously altered morphology or cell loss from the monolayer were observed in NIH-OVCAR3 cultures exposed for up to 48 hours to either type of nanoparticle at concentrations up to 75 µg/mL (Figure 1A). Of note, at this concentration, amine-modified polystyrene nanoparticles 1000 nm diameter were extremely toxic, underscoring the importance of nanoparticle size in cell toxicity (Figure 1A). Cell viability was further tested with CellTracker, a thiol-reactive probe that produces a stable membrane-impermeable glutathione-fluorescent dye adduct in metabolically active cells. CellTracker staining enables direct imaging of any metabolic injury in cells loaded with nanoparticles.[37] Based on the images in Figure 1B, after 48 hours of incubation, both mesoporous silica and polystyrene nanoparticles (at concentrations of 30 µg/mL and 75 µg/mL, respectively) exerted no toxic effects on ovarian cancer cell metabolism. This conclusion is supported by quantitative analysis using ImageJ software.

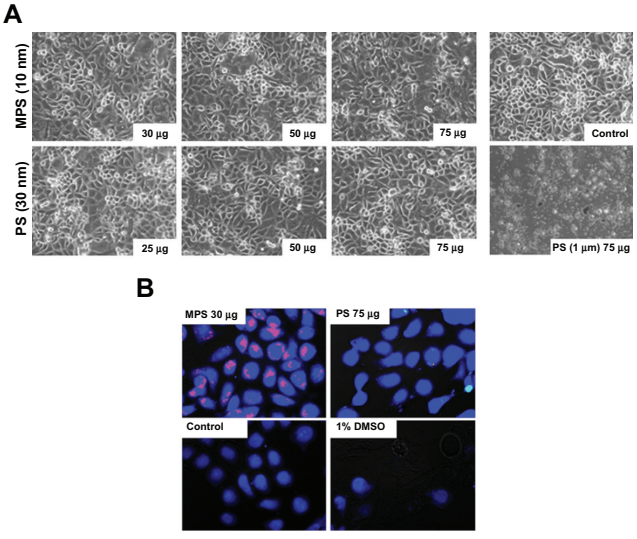

Figure 1 Biotolerability of nanoparticles. NIH-OVCAR3 cells adherent on coverslips were incubated with 10 nm naked mesoporous silica or 30 nm COOH-polystyrene nanoparticles (at the indicated concentration) in fresh medium for 48 hours. Thereafter, the monolayers were extensively washed to remove the excess of unbound nanoparticles and (**A**) imaged under the phase-contrast microscope to document gross morphological alterations or cell loss, and (**B**) labeled with CellTracker™ to show metabolic effects.
Note: Positive control of toxicity was performed by incubating the cells with 1% dimethyl sulfoxide.

The fluorescent signal in the images shown in Figure 1B indicates that the mesoporous silica nanoparticles accumulated in large quantities in NIH-OVCAR3 cells, while only a few cancer cells appeared to contain polystyrene nanoparticles, and in very small amounts. The latter finding could be explained on the basis that polystyrene nanoparticles hardly entered the cells, polystyrene-associated fluorescence was rapidly and fully quenched within the cellular compartments, or the polystyrene nanoparticles were extruded after internalization. On the other hand, mesoporous silica nanoparticles were also clearly detectable in cells when used at a very low concentration (0.5 µg/mL) and for a short duration of exposure (5 minutes, Figure 2A). In a typical dose-dependent uptake experiment, mesoporous silica nanoparticles were shown to almost saturate intracellular compartments after only 5 minutes of incubation, at doses starting from 5 µg/mL. Intracellular accumulation of mesoporous silica nanoparticles at 10 µg/mL did not increase with duration of incubation, whereas that of polystyrene nanoparticles (used at a concentration 7.5-fold that of mesoporous silica nanoparticles) increased greatly between 10 and 30 minutes of incubation, and a further slight increase occurred between 30 and 60 minutes (Figure 2B). Quantitative analysis with ImageJ software confirmed that while the mesoporous silica nanoparticles readily (within 30 minutes) saturated the intracellular compartments in almost 90% of the cell population, the polystyrene nanoparticles required a longer incubation time (>30 minutes) to reach a similar level of saturation (data not shown).

For objective measurement of endocytosis rates, we directly compared the uptake kinetics of mesoporous silica and polystyrene nanoparticles. At the end of each incubation time point, the samples were thoroughly washed to remove all noninternalized nanoparticles from the cell surface, quenched with Trypan blue, and then analyzed by flow cytometry to determine the fraction of cells that had internalized into the nanoparticles. An aliquot of washed cells was observed under the microscope to ascertain the absence of fluorescent nanoparticles passively adsorbed on the cell surface. Flow cytometry data were expressed as the percentage of fluorescently labeled cells. Both types of nanoparticles were taken up by

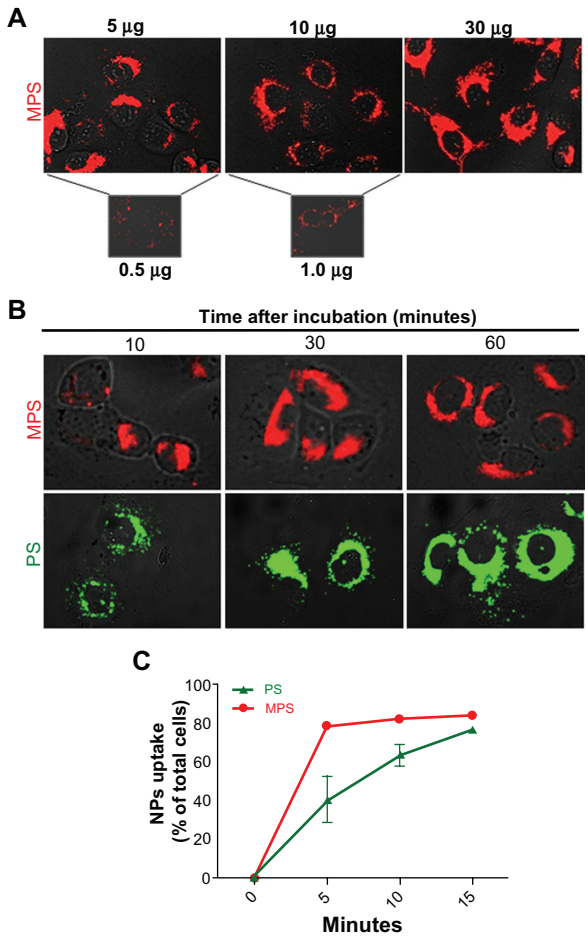

Figure 2 Dose-dependent and time-dependent cellular accumulation of nanoparticles. (**A**) Cells adherent on coverslips were exposed to different concentrations of 10 nm naked mesoporous silica nanoparticles for 5 minutes and imaged by fluorescence microscopy. (**B**) Adherent cells exposed to 10 µg/mL of 10 nm naked mesoporous silica nanoparticles or 75 µg/mL of COOH-polystyrene nanoparticles for the time indicated as imaged by fluorescence microscopy. (**C**) Cytofluorometric evaluation of labeled cells incubated with 10 µg/mL of 10 nm naked mesoporous silica nanoparticles or 75 µg/mL of 30 nm COOH-polystyrene nanoparticles for increasing periods of time.

the cells, although with differing degrees of efficiency. The mesoporous silica nanoparticles entered rapidly and 80% of the culture was saturated by 5 minutes, but less than 40% of the cell population was labeled by polystyrene nanoparticles at this time (Figure 2C). Saturation of approximately 80% of the cells with polystyrene nanoparticles was achieved within 15 minutes of incubation (Figure 2C).

The actual amount of nanoparticles accumulated in the cell results from the dynamic interplay between endocytosis and exocytosis. Therefore, we sought to assess the intracellular retention and exocytosis rates for mesoporous silica and polystyrene nanoparticles in ovarian cancer cells using a pulse-chase experiment. The cells were incubated with the nanoparticles for 15 minutes, ie, sufficient time to label the large majority of the cell population. The cells were then washed thoroughly and observed under the fluorescence microscope at intervals up to 120 minutes to assess visually the fluorescent signal retained in the cells. The images in Figure 3A show that the mesoporous silica nanoparticles persisted in the cells during 120 minutes of chase, whereas the fluorescent signal from the polystyrene nanoparticles in the cells rapidly (soon after 15 minutes of chase) dropped and became only faintly visible by 120 minutes. Quantification using ImageJ software confirmed that while the cell-associated fluorescent signal of the mesoporous silica nanoparticles remained essentially unchanged, the fluorescent signal from the polystyrene nanoparticles was reduced by some 80% after only 15 minutes of chase (data not shown). A parallel cytofluorometry experiment was conducted to quantify the proportion of cells labeled with nanoparticles. The results of this experiment corroborated the observation reported in Figure 3A. Flow cytometry data showed that more than 70% of the cells rapidly (within 15 minutes) lost the polystyrene nanoparticles, and by 120 minutes only about 5% of the cell population was still labeled with these nanoparticles. Accurate microscopic observation documented exocytosis of the polystyrene nanoparticles from cells after 30 minutes of chase. The image in Figure 3C shows the presence of polystyrene nanoparticles outside the cells, whereas those few remaining inside the cells are mainly located at the extreme periphery and beneath the plasma membrane, compatible with ongoing exocytosis. Taken together, these data indicate

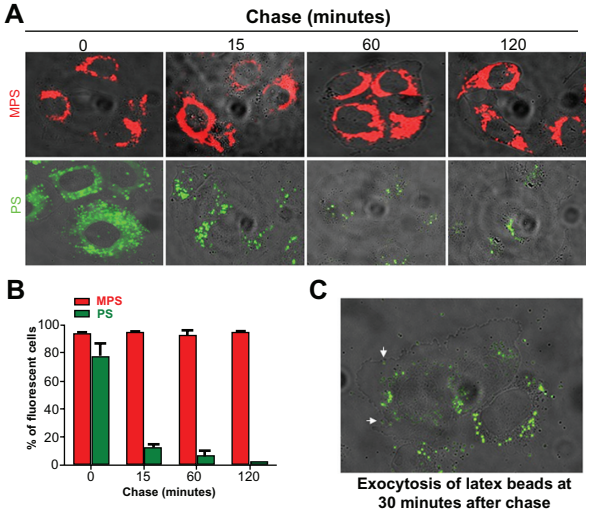

Figure 3 Mesoporous silica and polystyrene nanoparticles in ovarian cancer cells. (**A**) Adherent cells were incubated in fresh medium with 30 µg of 10 nm naked mesoporous silica or 75 µg of 30 nm COOH-polystyrene nanoparticles for 15 minutes. The cultures were then thoroughly washed, incubated in fresh medium, and imaged at the time indicated. (**B**) A parallel set of cultures treated as described in (**A**) was used to estimate cell-associated fluorescence by flow cytometry. (**C**) Cells incubated with 75 µg of polystyrene nanoparticles for 15 minutes, washed, and imaged after 30 minutes of tracking.

that polystyrene nanoparticles are actively extruded by ovarian cancer cells. A separate experiment demonstrated that mesoporous silica nanoparticles could instead label the cells for up to 72 hours (data not shown). Considering that the doubling-time of NIH-OVCAR3 cells under our experimental conditions is approximately 20.5 hours, our data indicate that, at saturating conditions, mesoporous silica nanoparticles are stably retained in ovarian cancer cells and can monitor cells for at least three generations.

Different intracellular traffic and final localization

Endocytosis brings extracellular material initially to early endosomes, then to late endosomes and, eventually, to lysosomes.[5] To see whether the mesoporous silica and polystyrene nanoparticles converged into the same intracellular compartments after internalization, we coincubated ovarian cancer cells with these nanoparticles and followed their intracellular traffic and localization at increasing chase times. The cells were exposed to the nanoparticles at saturating conditions (30 μg/mL mesoporous silica and 75 μg/mL polystyrene, 15 minutes of incubation). The monolayer was then promptly and thoroughly washed three times with abundant phosphate-buffered solution and further incubated in fresh culture medium for up to 120 minutes. At intervals, a coverslip was taken and the monolayer was imaged by fluorescence microscopy (Figure 4A). Mesoporous silica nanoparticles stably localized in the perinuclear region showing typical compartmentalized features in the first 30 minutes of chase and cytoplasmic localization in the subsequent period of incubation (Figure 4A). Polystyrene nanoparticles were clearly visible in the first 30 minutes of tracking, but were no longer detectable in the cells by 120 minutes of tracking (Figure 4A). Polystyrene nanoparticles showed punctuate fluorescence, compatible with intravesicular accumulation, which was mainly localized at the extreme periphery of the cells (Figure 4A).

It is noteworthy that the mesoporous silica and polystyrene nanoparticles never merged, indicating that the two types of nanoparticles followed different endocytic routes. To characterize the endocytic pathways of mesoporous silica and polystyrene nanoparticles, we performed a kinetic study of their uptake and intracellular trafficking using Lysotracker as a fluorescent tracer of internalization and of intracellular acid compartments. To obtain an objective evaluation of the labeled vesicles, the two fluorescent signals were quantified as individual or merged spots using ImageJ software.

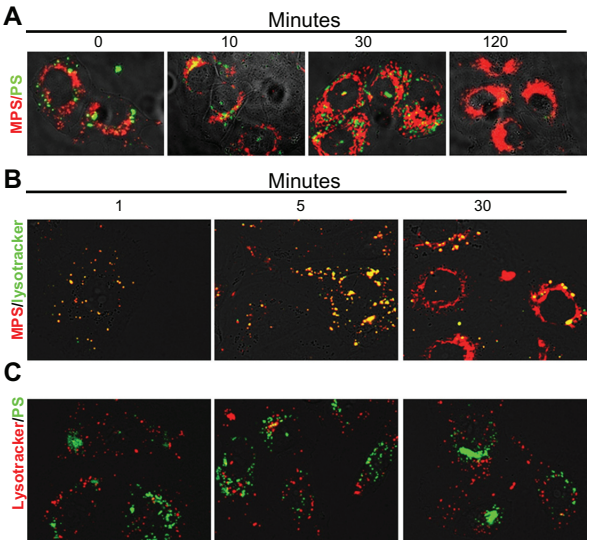

Figure 4 Mesoporous silica and polystyrene nanoparticles take different endocytic routes and localize to distinct intracellular compartments. (**A**) Cells adherent on coverslips were coincubated for 5 minutes with 30 μg of 10 nm naked mesoporous silica nanoparticles and 75 μg of 30 nm COOH-polystyrene nanoparticles. The cells were then washed and imaged at 0, 10, 30, and 120 minutes of trace. (**B** and **C**) Cells adherent on coverslips were preincubated for 10 minutes with Lysotracker Green or Red, then washed and incubated with nanoparticles (as indicated), and imaged at 1, 5, and 30 minutes.

Preliminary experiments indicated that endocytosis and intracellular vesicular redistribution of nanoparticles were very rapid events. The cells were preloaded with Lysotracker for 10 minutes to allow complete labeling of vesicles along the endocytic pathway downstream from the lysosomes. Excess Lysotracker was washed out, and the cells were labeled with nanoparticles and observed under the fluorescence microscope at one, 5, and 30 minutes of incubation (note that approximately 60–90 seconds were required for extensive washing with cold buffer solution and mounting before capturing the images). Five to ten fields chosen at random were imaged for each sample. Representative images are shown in Figure 4B (for mesoporous silica nanoparticles) and in Figure 4C (for polystyrene nanoparticles). Digitalized images were then analyzed for quantification using ImageJ software. Mesoporous silica and Lysotracker showed almost complete (94% ± 2%) colocalization at one and 5 minutes after labeling and became partially separated by 30 minutes. Quantification of cell-associated fluorescence showed that more than 98% Lysotracker-positive vesicles were also labeled with mesoporous silica nanoparticles at this time, while more 90% of mesoporous silica fluorescence was not merged with Lysotracker fluorescence. The latter observation could reflect loss of signal from Lysotracker Green or a physical separation of the two tracers. Indeed, the overall fluorescence emission of Lysotracker Green diminished with

incubation time. Still, the diffuse localization of mesoporous silica fluorescence in the cell favors the interpretation that, with time, the 10 nm mesoporous silica nanoparticles abandoned the acid compartments. Strikingly, at any time, polystyrene nanoparticles colocalized with Lysotracker Red (Figure 4C). From these data, we conclude that mesoporous silica and polystyrene nanoparticles follow different endocytic routes and reach different final compartments in the cell.

Different endocytic mechanisms

The observed differences in internalization and retention rates of mesoporous silica and polystyrene nanoparticles may reflect differences in uptake mechanisms dictated by specific physicochemical properties of the nanoparticles. Alternatively, mesoporous silica and polystyrene nanoparticles could enter the cell via a common endocytosis mechanism and thereafter be sorted into different populations of endocytic vesicles.[38] We first checked whether uptake of the nanoparticles occurred passively or required energy. To this end, we compared the internalization of mesoporous silica and polystyrene nanoparticles at 4°C and 37°C. In a typical experiment, the cells were incubated for 30 minutes at 4°C with saturating concentrations of mesoporous silica (30 μg/mL) or polystyrene (75 μg/mL) nanoparticles. Thereafter, the cells were kept at 37°C and internalization was assessed by microscopic imaging at increasing time points (Figure 5A). A parallel set of cultures was incubated for 30 minutes at 37°C to serve as a standard control for uptake efficiency (Figure 5B). ImageJ software was used for quantification. At 0 minutes after recovery at 37°C, the uptake of mesoporous silica nanoparticles in culture incubated at 4°C was reduced to 90% ± 3% compared with that observed in control cultures (assumed to be 100%). Internalization of mesoporous silica nanoparticles increased with duration of incubation at 37°C, reaching values of 15% ± 3%, 45% ± 5%, and 75% ± 5% of control at 5, 10, and 30 minutes, respectively (Figure 5A). The uptake of polystyrene nanoparticles was apparently not affected by low temperature. In fact, the cell-associated fluorescence of the polystyrene nanoparticles was comparable in cultures incubated at 37°C (controls, Figure 5B) and at 4°C (time 0 minutes), and also after recovery at 37°C (Figure 5A).

To obtain further objective quantification of temperature-dependent uptake of the nanoparticles, a parallel set of cultures was analyzed by cytofluorometry. The data shown in Figure 5C confirm that the uptake of polystyrene nanoparticles was not impaired during incubation at 4°C followed by recovery at 37°C (compared with uptake at 37°C,

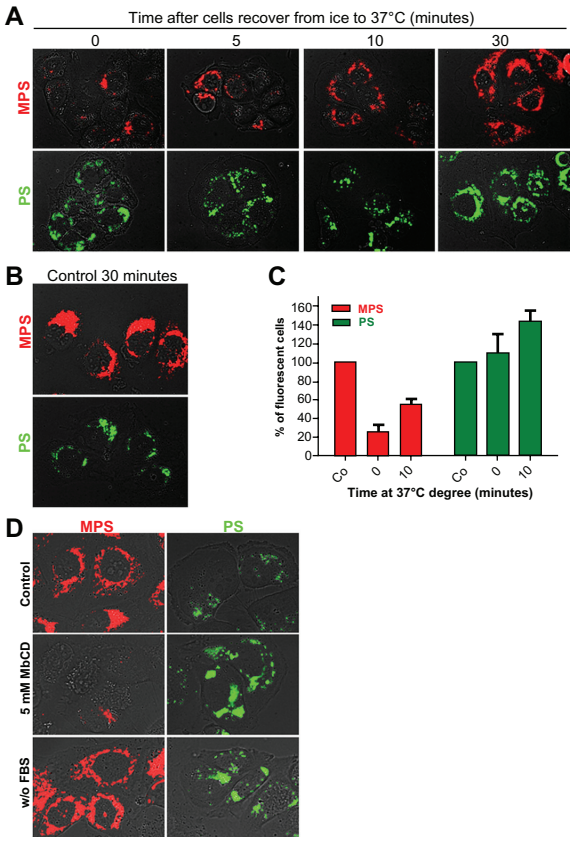

Figure 5 Energy-temperature dependence of nanoparticle endocytosis. (**A**) Cells adherent on coverslips were incubated for 30 minutes in the presence of 30 μg of 10 nm naked mesoporous silica or 75 μg of 30 nm COOH-polystyrene nanoparticles at 4°C (on ice). The cells were then washed thoroughly, incubated at 37°C, and imaged at the time indicated. (**B**) Control cells were incubated for 30 minutes at 37°C with 30 μg of mesoporous silica or 75 μg of polystyrene nanoparticles. (**C**) A parallel set of cultures treated as described in panel A was used for flow cytometry evaluation of cell-associated fluorescence. (**D**) NIH-OVCAR cells adherent on coverslips were pulse-labeled for 15 minutes with 10 μg of 10 nm naked mesoporous silica or 75 μg of 30 nm COOH-polystyrene nanoparticles in complete or serum-free medium as indicated.

Note: Parallel cultures preincubated for one hour with 5 mM methyl-β-cyclodextrin in serum-free medium were used to assess clathrin/caveolae-mediated endocytosis.

assumed to be 100%), while that of the mesoporous silica nanoparticles was reduced by some 80% at time 0 minutes and reached 50% of control values 10 minutes after recovery at 37°C. We further investigated the mechanism by which the nanoparticles gained entry into the ovarian cancer cells. Cholesterol in the plasma membrane has been shown to be involved in various cellular uptake mechanisms, including those mediated by clathrin, caveolae, and lipid rafts.[39] These endocytic pathways can be disrupted by selective extraction of cholesterol from the plasma membrane imparted by MbCD.[40] We sought to define whether mesoporous silica and polystyrene nanoparticles exploited a cholesterol-dependent mechanism of cellular entry. NIH-OVCAR3 cells were or were not preincubated for 60 minutes in serum-free medium containing 5 mM MbCD, a condition sufficient to deplete

the plasma membrane of cholesterol. The cells were then pulsed for 15 minutes with either type of nanoparticle and, after thorough washing, were rapidly observed and imaged under the fluorescence microscope. In the control serum-containing medium, uptake and internal accumulation of both nanoparticles in NIH-OVCAR3 cells resembled our previous findings, being more efficient for mesoporous silica (Figure 5D). Under membrane cholesterol-depleted conditions, the uptake of mesoporous silica nanoparticles was almost completed prevented, while that of polystyrene nanoparticles appeared to be greatly stimulated (Figure 5D). It should be noted that incubation in serum-deprived medium greatly stimulated the uptake of polystyrene nanoparticles, while this condition did not modify the uptake efficiency of mesoporous silica nanoparticles (Figure 5D).

Size and charged functional groups affect biocompatibility

Finally, we tested the biocompatibility, uptake, and intracellular compartmentalization of mesoporous silica and polystyrene nanoparticles 50 nm in diameter with or without charged functional groups on the surface. The uptake and retention efficiency of the nanoparticles, as well as their intracellular trafficking, also depend heavily on intrinsic cell characteristics, mainly the composition and fluidity of the plasma membrane, and the dynamics of endocytosis and exocytosis.[41] The above data demonstrate the relevance of cholesterol in the plasma membrane to endocytosis of nanoparticles. Plasma membrane cholesterol is a major constituent of caveolae, ie, invaginated regions of the plasma membrane that accomplish caveolin-1-dependent endocytosis. To determine the involvement of caveolin-1 in the nanoparticle uptake mechanism, in this set of experiments we included the SKOV3 ovarian cancer cell line. As shown by Western blotting, SKOV3 cells highly express caveolin-1, whereas this protein is undetectable in NIH-OVCAR3 cells (Figure 6A). When the 50 nm polystyrene nanoparticles functionalized with NH_2 groups were applied to ovarian cancer cultures, cytotoxicity became apparent after 4–8 hours (depending on the dose, data not shown). A short incubation period (15 minutes) was sufficient to reveal that these nanoparticles entered the cells rapidly and accumulated within Lysotracker-positive acid compartments (Figure 6B). In contrast, the 30 nm COOH-functionalized polystyrene nanoparticles continuously added to the culture for 24 hours entered both SKOV3 and NIH-OVCAR3 cells with similar efficiency, thus showing independence from caveolin-1 expression (Figure 6C). These nanoparticles

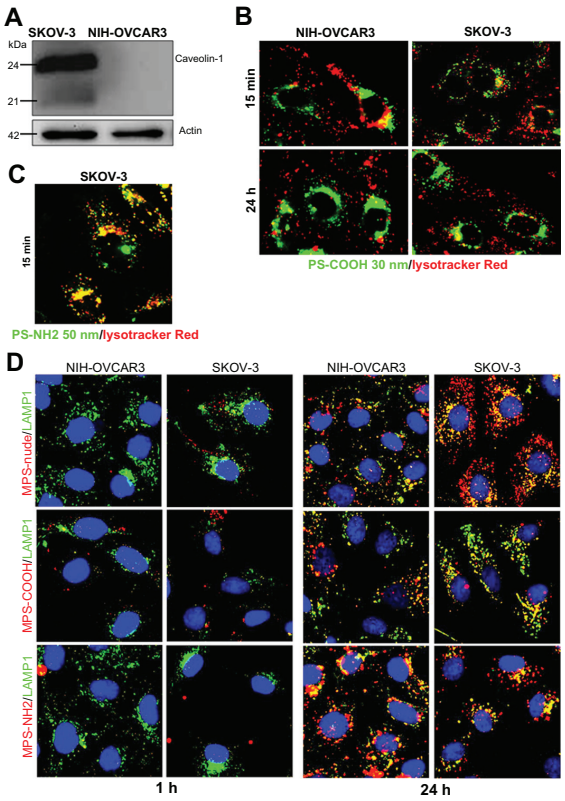

Figure 6 Size and charged functional groups differentially affect the uptake and biocompatibility of mesoporous silica and polystyrene nanoparticles in ovarian cancer cells expressing or not expressing caveolin-1. (**A**) Western blotting of caveolin-1 in NIH-OVCAR3 and SKOV3 cells. The filter was reprobed for actin as a reference protein for loading of the lanes. The molecular weight of the proteins is indicated. Data were reproduced in three independent experiments. (**B**) Colocalization of 50 nm amine-modified polystyrene nanoparticles with Lysotracker-positive acid compartments in SKOV3 cells after an incubation time of 15 minutes with 75 μg of nanoparticles. (**C**) Comparison of uptake and intracellular localization of 30 nm COOH-polystyrene nanoparticles in SKOV3 and NIH-OVCAR cells after incubation times of one and 24 hours with 75 μg of nanoparticles. The 30 nm COOH-polystyrene nanoparticles showed no colocalization with the acid compartment tracer, Lysotracker Red. (**D**) Comparison of uptake and intracellular localization of 50 nm mesoporous silica nanoparticles functionalized or not with either COOH or NH_2 groups in SKOV3 and NIH-OVCAR cells after incubation times of one and 24 hours with 20 μg of nanoparticles.
Note: Endosomal and lysosomal compartments were identified using the Lamp-1 antibody.

were not toxic, even after 24 hours of continuous incubation. It is noteworthy that, unlike the 50 nm NH_2-polystyrene nanoparticles, the 30 nm COOH-polystyrene nanoparticles never showed overlap with the Lysotracker tracer in the acid compartments during 24 hours of incubation, either in SKOV3 or in NIH-OVCAR3 cells (Figure 6C). These data are in agreement with the data shown in Figure 4, and confirm that uptake of 30 nm polystyrene nanoparticles also occurs independently of caveolin-1 and does not follow the classic acidic endocytosis pathway.

Next, we focused on mesoporous silica nanoparticles. Compared with their 10 nm counterparts, the 50 nm naked mesoporous silica nanoparticles entered the

NIH-OVCAR3 cells at a very low rate (Figure 6D). SKOV3 cells were more likely to take up these nanoparticles (Figure 6D). With regard to surface chemistry, the carboxyl-modified mesoporous silica nanoparticles showed the least entry efficiency in both cell lines (Figure 6D). Altogether, the data in Figure 6D indicate that increasing the size from 10 nm to 50 nm reduces the uptake efficiency of mesoporous silica nanoparticles, negatively charged surface groups impair endocytosis of mesoporous silica nanoparticles, regardless of the presence or absence of caveolin-1 on the plasma membrane, and 50 nm mesoporous silica nanoparticles enter and reside permanently in lysosomes.

Discussion

The ideal theranostic nanoparticle is not toxic in itself, is biocompatible and biodegradable, is easily and efficiently taken up and retained within the cell for the time needed to exert its diagnostic and therapeutic function, and safely reaches the intracellular compartment of the cancer cell where it can release its cytotoxic drug cargo.[12] Uptake, intracellular trafficking, and biotolerability of nanoparticles are greatly influenced by type of material, shape, size, and surface charge.[23,42] Size is particularly critical for intracellular trafficking and the final destination of endocytosed nanoparticles, given that endocytic compartments range between 300 nm and 1000 nm.[5] Both the 1000 nm and 50 nm amine-modified polystyrene nanoparticles were toxic to ovarian cancer cells, while 10 nm and 50 nm mesoporous silica and 30 nm carboxyl-modified polystyrene nanoparticles exerted no toxic effects on metabolism in ovarian cancer cells, consistent with previous reports showing the biotolerability of mesoporous silica[19,30,37,43] and carboxylated polystyrene[27,29,44] nanoparticles in other cell types. The potentially deleterious effects of nanoparticles on cell metabolism depend on their physicochemical characteristics, uptake efficiency, and final intracellular destination, as well as their accumulation in critical compartments. We found that naked mesoporous silica and negatively charged polystyrene-COOH nanoparticles were endocytosed and retained by NIH-OVCAR3 cells with variable efficiency. The 10 nm mesoporous silica nanoparticles showed clear vesicular localization when used at low doses (up to 1 μg/mL), and accumulated in the cytoplasm when used at higher concentrations and for longer than 30 minutes, suggesting that once the 10 nm nanoparticles have saturated the endosomal-lysosomal compartments, leakage toward the cytosol may occur. However, 50 nm mesoporous silica nanoparticles entered with much lower efficiency and localized permanently in lysosomes. On the other hand, polystyrene nanoparticles temporarily accumulated in recycling endocytic vesicles and therefore showed limited intracellular accumulation. The two types of nanoparticles never showed overlap of the endocytic routes, in that while the mesoporous silica nanoparticles transited through acid compartments labeled by Lysotracker, COOH-polystyrene nanoparticles followed an endocytic route not labeled by Lysotracker. These findings suggest that the two types of nanoparticles had different endocytic mechanisms and routes which led them to distinct subcellular compartments. Lowering the temperature to approximately 4°C completely inhibited the uptake of mesoporous silica nanoparticles but not that of polystyrene nanoparticles, indicating that entry of the former was energy-dependent.

To investigate further the mechanism of nanoparticle internalization, we used MbCD, which depletes the plasma membrane of cholesterol and thus inhibits clathrin-mediated and caveolin-mediated endocytosis.[39] Uptake of mesoporous silica nanoparticles was largely prevented when the cholesterol-dependent endocytic mechanism was disrupted, while that of polystyrene nanoparticles apparently increased. Because MbCD treatment was given in the absence of serum, this increase can be explained with the "protein corona" effect.[45] This effect consists of reduced internalization of nanoparticles due to adsorption of serum protein on the surface of the nanoparticle. In effect, uptake of polystyrene nanoparticles, but not that of mesoporous silica nanoparticles, was higher in the absence of serum than in its presence.

The present data are fully in agreement with a recent report by Smith et al.[29] Size and surface chemistry have been shown to be important characteristics influencing the efficiency and mechanism of uptake in various cells.[44,46–51] COOH-polystyrene nanoparticles with a diameter < 200 nm showed reduced cell surface binding in the presence of serum,[52] which results in low uptake efficiency.[51] Accordingly, it has recently been shown that cellular association and endocytosis of 20 nm COOH-polystyrene nanoparticles is greatly reduced in the presence of serum.[29] It has also been shown that regardless of the presence or absence of serum, 20 nm COOH-polystyrene nanoparticles enter cells via clathrin-mediated endocytosis.[29] The 30 nm COOH-polystyrene nanoparticles were very efficiently taken up by SKOV3 cells regardless of whether incubation was performed in the presence or absence of serum or under membrane cholesterol-depleted conditions (data not shown). Thus, in SKOV3 cells, the serum "protein corona" did not interfere with the mechanism of entry, and the cholesterol-dependent endocytic pathway

Table 1 Physicochemical characteristics and biological properties of the nanoparticles used in this study

NPs	Material	Size (nm)	Surface functional group	Toxicity	Cholesterol-dep uptake	Protein corona effect	Cell compartmentalization
MPS	Mesoporous silica	10	None	No	Yes	No	Lysosome → cytosol
MPS	Mesoporous silica	50	None	No	Yes	No	Lysosome
MPS	Mesoporous silica	50	–NH2	No	Yes	ND	Lysosome
MPS	Mesoporous silica	50	–COOH	No	Yes	ND	Lysosome
PS	Polystyrene	1000	–NH2	Yes	ND	ND	Lysosome
PS	Polystyrene	50	–NH2	Yes	ND	ND	Lysosome
PS	Polystyrene	30	–COOH	No	No	Yes	Recycling vesicles

was not involved in the uptake of polystyrene nanoparticles. This latter observation is in agreement with the findings of Fazlollalhi et al,[53] who showed that transcytosis of polystyrene nanoparticles in differentiated MDCK-II cells was not mediated by lipid-raft endocytosis. Moreover, uptake of 24 nm polystyrene nanoparticles by HeLa and human umbilical vein endothelial cells was also shown not to be dependent on clathrin or caveolae.[26] Consistent with our findings, the 30 nm polystyrene nanoparticles in these cells were found in recycling vesicles and not labeled with Lysotracker.[26]

Conclusion

In this work, we compared the biotolerability, uptake efficiency, and intracellular trafficking of mesoporous silica and polystyrene nanoparticles in cultured ovarian cancer cells. This was a pilot study to test the potential for use of these nanoparticles as theranostic vehicles in the diagnosis and treatment of ovarian cancer.[33] The principal findings of this study are schematically reported in Table 1. We have shown how the size and surface charge on the chemical groups of mesoporous silica and polystyrene nanoparticles differentially affect uptake, intracellular localization and retention, and biocompatibility in ovarian cancer cell lines expressing (SKOV-3) or not expressing (NIH-OVCAR3) caveolin-1. Endocytosis of COOH-polystyrene 30 nm nanoparticles did not follow the classic acid compartment pathway and entered recycling vesicles from which the nanoparticles were extruded, while the 50 nm amine-modified polystyrene nanoparticles accumulated within Lamp-1-positive acid compartments, and eventually (after incubation for longer than 8 hours) caused cell death. Mesoporous silica nanoparticles 10 nm in size rapidly entered the acid compartments and eventually accumulated in the cytoplasm, whereas 50 nm mesoporous silica nanoparticles permanently resided within lysosomes. Internalization of mesoporous silica nanoparticles was energy-dependent and cholesterol-dependent, and was in general (with the exception of COOH-modified nanoparticles) more efficient in SKOV3 cells than in NIH-OVCAR3 cells, underscoring the role of caveolin-1 in the uptake mechanism. It is to be noted that caveolin-1 is depleted or downregulated in the vast majority of ovarian carcinomas.[34] Therefore, choice of the most suitable nanotheranostics for targeting cancer cells should take into account the physicochemical characteristics of the nanoparticles in relation to the biochemical characteristics of the cell membrane.

Acknowledgments

This research was supported by Poli di Innovazione (Polo "Biotecnologie e Biomedicale", Progetto BANP, FinPiemonte, Italy). The fluorescence optical imaging facility was sponsored by Comoli, Ferrari, and C SpA (Novara, Italy). ME was supported with a fellowship from Regione Piemonte, Italy.

Disclosures

Cyanine Technology SpA (Turin, Italy) provided the IRIS-3-doped mesoporous silica nanoparticles free of charge. AG is the recipient of a PhD fellowship partly financed by Cyanine Technologies SpA. Authors have no further conflicts of interest to disclose.

References

1. Jemal A, Bray F, Center MM, Ferlay J, Ward E, Forman D. Global cancer statistics. *CA Cancer J Clin*. 2011;61:69–90.
2. Clarke-Pearson DL. Clinical practice. Screening for ovarian cancer. *N Engl J Med*. 2009;361:170–177.
3. Liu JR, Opipari AW, Tan L, et al. Dysfunctional apoptosome activation in ovarian cancer: implications for chemoresistance. *Cancer Res*. 2002;62:924–931.
4. Mezzanzanica D, Canevari S, Cecco LD, Bagnoli M. miRNA control of apoptotic programs: focus on ovarian cancer. *Expert Rev Mol Diagn*. 2011;11:277–286.

5. Castino R, Démoz M, Isidoro C. Destination 'lysosome': a target organelle for tumour cell killing? *J Mol Recognit*. 2003;16:337–348.
6. Duvvuri M, Krise JP. Intracellular drug sequestration events associated with the emergence of multidrug resistance: a mechanistic review. *Front Biosci*. 2005;10:1499–1509.
7. Krishna R, Mayer LD. Multidrug resistance (MDR) in cancer. Mechanisms, reversal using modulators of MDR and the role of MDR modulators in influencing the pharmacokinetics of anticancer drugs. *Eur J Pharm Sci*. 2000;11:265–283.
8. Chen T, Shukoor MI, Wang R, et al. Smart multifunctional nanostructure for targeted cancer chemotherapy and magnetic resonance imaging. *ACS Nano*. 2011;5:7866–78673.
9. Lammers T, Aime S, Hennink WE, Storm G, Kiessling F. Theranostic nanomedicine. *Acc Chem Res*. 2011;44:1029–1038.
10. Caldorera-Moore ME, Liechty WB, Peppas NA. Responsive theranostic systems: integration of diagnostic imaging agents and responsive controlled release drug delivery carriers. *Acc Chem Res*. 2011;44:1061–1070.
11. Kievit FM, Zhang M. Cancer nanotheranostics: improving imaging and therapy by targeted delivery across biological barriers. *Adv Mater*. 2011;23:H217–H247.
12. Shapira A, Livney YD, Broxterman HJ, Assaraf YG. Nanomedicine for targeted cancer therapy: towards the overcoming of drug resistance. *Drug Resist Updat*. 2011;14:150–163.
13. Iyer AK, Khaled G, Fang J, Maeda H. Exploiting the enhanced permeability and retention effect for tumor targeting. *Drug Discov Today*. 2006;11:812–818.
14. Wang M, Thanou M. Targeting nanoparticles to cancer. *Pharmacol Res*. 2010;62:90–99.
15. Ruoslahti E, Bhatia SN, Sailor MJ. Targeting of drugs and nanoparticles to tumors. *J Cell Biol*. 2010;188:759–768.
16. Lei T, Srinivasan S, Tang Y, et al. Comparing cellular uptake and cytotoxicity of targeted drug carriers in cancer cell lines with different drug resistance mechanisms. *Nanomedicine*. 2011;7:324–332.
17. Ferris DP, Lu J, Gothard C, et al. Synthesis of biomolecule-modified mesoporous silica nanoparticles for targeted hydrophobic drug delivery to cancer cells. *Small*. 2011;7:1816–1826.
18. Benezra M, Penate-Medina O, Zanzonico PB, et al. Multimodal silica nanoparticles are effective cancer-targeted probes in a model of human melanoma. *J Clin Invest*. 2011;121:2768–2780.
19. Rosenholm JM, Meinander A, Peuhu E, et al. Targeting of porous hybrid silica nanoparticles to cancer cells. *ACS Nano*. 2009;3:197–206.
20. Lee S, Yun HS, Kim SH. The comparative effects of mesoporous silica nanoparticles and colloidal silica on inflammation and apoptosis. *Biomaterials*. 2011;32:9434–9443.
21. Wang T, Zhang L, Su Z, Wang C, Liao Y, Fu Q. Multifunctional hollow mesoporous silica nanocages for cancer cell detection and the combined chemotherapy and photodynamic therapy. *ACS Appl Mater Interfaces*. 2011;3:2479–2486.
22. Ye Y, Liu J, Xu J, Sun L, Chen M, Lan M. Nano-SiO_2 induces apoptosis via activation of p53 and Bax mediated by oxidative stress in human hepatic cell line. *Toxicol In Vitro*. 2010;24:751–758.
23. Lu X, Qian J, Zhou H, et al. In vitro cytotoxicity and induction of apoptosis by silica nanoparticles in human HepG2 hepatoma cells. *Int J Nanomedicine*. 2011;6:1889–1901.
24. Corbalan JJ, Medina C, Jacoby A, Malinski T, Radomski MW. Amorphous silica nanoparticles trigger nitric oxide/peroxynitrite imbalance in human endothelial cells: inflammatory and cytotoxic effects. *Int J Nanomedicine*. 2011;6:2821–2835.
25. Giri S, Trewyn BG, Lin VS. Mesoporous silica nanomaterial-based biotechnological and biomedical delivery systems. *Nanomedicine (Lond)*. 2007;2:99–111.
26. Lai SK, Hida K, Man ST, et al. Privileged delivery of polymer nanoparticles to the perinuclear region of live cells via a non-clathrin, non-degradative pathway. *Biomaterials*. 2007;28:2876–2884.
27. Lunov O, Syrovets T, Loos C, et al. Differential uptake of functionalized polystyrene nanoparticles by human macrophages and a monocytic cell line. *ACS Nano*. 2011;5:1657–1669.
28. Yanagisawa R, Takano H, Inoue KI, Koike E, Sadakane K, Ichinose T. Size effects of polystyrene nanoparticles on atopic dermatitis-like skin lesions in NC/NGA mice. *Int J Immunopathol Pharmacol*. 2010;23:131–141.
29. Smith P, Giroud M, Wiggins E, et al. Cellular entry of nanoparticles via serum sensitive clathrin-mediated endocytosis, and plasma membrane permeabilization. *Int J Nanomedicine*. 2012;7:2045–2055.
30. Gianotti E, Bertolino CA, Benzi C, et al. Photoactive hybrid nanomaterials: indocyanine immobilized in mesoporous MCM-41 for "in-cell" bioimaging. *ACS Appl Mater Interfaces*. 2009;1:678–687.
31. Castino R, Peracchio C, Salini A, et al. Chemotherapy drug response in ovarian cancer cells strictly depends on a cathepsin D-Bax activation loop. *J Cell Mol Med*. 2009;13:1096–1109.
32. Straubinger RM, Lopez NG, Debs RJ, Hong K, Papahadjopoulos D. Liposome-based therapy of human ovarian cancer: parameters determining potency of negatively charged and antibody-targeted liposomes. *Cancer Res*. 1988;48:5237–5245.
33. Hamelers IH, Staffhorst RW, Voortman J, et al. High cytotoxicity of cisplatin nanocapsules in ovarian carcinoma cells depends on uptake by caveolae-mediated endocytosis. *Clin Cancer Res*. 2009;15:1259–1268.
34. Wiechen K, Diatchenko L, Agoulnik A, et al. Caveolin-1 is down-regulated in human ovarian carcinoma and acts as a candidate tumor suppressor gene. *Am J Pathol*. 2001;159:1635–1643.
35. Burghardt RC, Barhoumi R, Lewis EH, et al. Patulin-induced cellular toxicity: a vital fluorescence study. *Toxicol Appl Pharmacol*. 1992;112:235–244.
36. Castino R, Fiorentino I, Cagnin M, Giovia A, Isidoro C. Chelation of lisosomal iron protects dopaminergic SH-SY5Y neuroblastoma cells from hydrogen peroxide toxicity by precluding autophagy and Akt dephosphorylation. *Toxicol Sci*. 2011;123:523–541.
37. Ekkapongpisit M, Giovia A, Nicotra G, Ozzano M, Caputo G, Isidoro C. Labeling and exocytosis of secretory compartments in RBL mastocytes by polystyrene and mesoporous silica nanoparticles. *Int J Nanomedicine*. 2012;7:1829–1840.
38. Lakadamyali M, Rust MJ, Zhuang X. Ligands for clathrin-mediated endocytosis are differentially sorted into distinct populations of early endosomes. *Cell*. 2006;124:997–1009.
39. Pichler H, Riezman H. Where sterols are required for endocytosis. *Biochim Biophys Acta*. 2004;1666:51–61.
40. Kilsdonk EP, Yancey PG, Stoudt GW, et al. Cellular cholesterol efflux mediated by cyclodextrins. *J Biol Chem*. 1995;270:17250–17256.
41. Dombu CY, Kroubi M, Zibouche R, Matran R, Betbeder D. Characterization of endocytosis and exocytosis of cationic nanoparticles in airway epithelium cells. *Nanotechnology*. 2010;21:355102.
42. Park MV, Neigh AM, Vermeulen JP, et al. The effect of particle size on the cytotoxicity, inflammation, developmental toxicity and genotoxicity of silver nanoparticles. *Biomaterials*. 2011;32:9810–9817.
43. Lu J, Liong M, Zink JI, Tamanoi F. Mesoporous silica nanoparticles as a delivery system for hydrophobic anticancer drugs. *Small*. 2007;3:1341–1346.
44. Xia T, Kovochich M, Liong M, Zink JI, Nel AE. Cationic polystyrene nanosphere toxicity depends on cell-specific endocytic and mitochondrial injury pathways. *ACS Nano*. 2008;2:85–96.
45. Gessner A, Lieske A, Paulke BR, Müller RH. Functional groups on polystyrene model nanoparticles: influence on protein adsorption. *J Biomed Mater Res A*. 2003;65:319–326.
46. Nel AE, Mädler L, Velegol D, et al. Understanding biophysicochemical interactions at the nano-bio interface. *Nat Mater*. 2009;8:543–557.
47. Dausend J, Musyanovych A, Dass M, et al. Uptake mechanism of oppositely charged fluorescent nanoparticles in HeLa cells. *Macromol Biosci*. 2008;8:1135–1143.
48. Rejman J, Oberle V, Zuhorn IS, Hoekstra D. Size-dependent internalization of particles via the pathways of clathrin- and caveolae-mediated endocytosis. *Biochem J*. 2004;377:159–169.
49. Johnston HJ, Semmler-Behnke M, Brown DM, Kreyling W, Tran L, Stone V. Evaluating the uptake and intracellular fate of polystyrene nanoparticles by primary and hepatocyte cell lines in vitro. *Toxicol Appl Pharmacol*. 2010;242:66–78.

50. dos Santos T, Varela J, Lynch I, Salvati A, Dawson KA. Effects of transport inhibitors on the cellular uptake of carboxylated polystyrene nanoparticles in different cell lines. *PLoS One*. 2011;6:e24438.
51. Merhi M, Dombu CY, Brient A, et al. Study of serum interaction with a cationic nanoparticle: Implications for in vitro endocytosis, cytotoxicity and genotoxicity. *Int J Pharm*. 2012;423:37–44.
52. Baier G, Costa C, Zeller A, et al. BSA adsorption on differently charged polystyrene nanoparticles using isothermal titration calorimetry and the influence on cellular uptake. *Macromol Biosci*. 2011;11:628–638.
53. Fazlollahi F, Angelow S, Yacobi NR, et al. Polystyrene nanoparticle trafficking across MDCK-II. *Nanomedicine*. 2011;7:588–594.